Front. Mater. Sci. 2025, 19(2): 250725
https://doi.org/10.1007/s11706-025-0725-0

RESEARCH ARTICLE

Nano-imprinted cellulose acetate structures for light management of dye-sensitized solar cells

Maryam Esmaeilzadeh[1,2], Joice Kaschuk[3], Hoang M. Nguyen[4], Emilia Palo[1], Yazan Al Haj[4], Jaana Vapaavuori[4], and Kati Miettunen (✉)[1]

1 Department of Mechanical and Materials Engineering, Faculty of Technology, University of Turku, Turku, Finland
2 Department of Chemistry, Faculty of Science, University of Turku, Turku, Finland
3 Physical Chemistry and Soft Matter, Wageningen University & Research, 6708WE, Wageningen, Netherlands
4 Department of Chemistry and Materials Science, School of Chemical Engineering, Aalto University, Espoo, Finland

ABSTRACT: Advanced materials with surface patterning can improve light management in optoelectronic devices. In this work, we employed nanoimprinting lithography (NIL) using a hard polydimethylsiloxane (PDMS) mold to fabricate two-dimensional periodically structured films from cellulose acetate (CA). This periodic structure was selected to scatter the light to increase its optical path. The mold features translated well to the patterned CA films, as shown by scanning electron microscopy and atomic force microscopy analyses. The films showed an average peak-to-peak distance of (750 ± 40) nm and an average height of grooves of (130 ± 7) nm. Optical characterization confirmed a high transparency (> 90%) in the studied 300–800 nm range. These patterned cellulose films were applied atop dye solar cells to enhance light harvesting and improve device efficiency. The application of these films increased the average short-circuit current density by 17% ± 3% and efficiency by 18% ± 2% of the solar devices. Our results underscore that the easy and accessible NIL method can help develop patterned cellulose films for facile light-management patterning for optoelectronic device technologies.

KEYWORDS: nanoimprinting lithography; light scattering; photovoltaic; cellulose acetate

Contents

Received December 22, 2024; accepted April 8, 2025

E-mail: kati.miettunen@utu.fi

References

1 Introduction

Cellulose is an interesting upcoming material for photovoltaic and electronic applications due to its excellent optical properties, low cost, non-toxicity, and renewability [1–3]. In addition, cellulose materials exhibit strong resistance to optical alterations under prolonged periods of visible and ultraviolet (UV) light exposure, making them well-suited for such applications [4]. However, their stability in water remains a challenge. To address this, either material modifications are needed to improve water resistance, or applications should be targeted where moisture exposure is minimal, such as indoor environments.

Among cellulose materials, cellulose acetate (CA) is a widely used cellulose derivative that has higher hydrophobicity compared to other cellulose types [5], and it is soluble in common organic solvents, such as acetone, to make transparent films [6–7]. Transparent cellulose materials are promising alternatives for conventional substrates such as glass and polymers (e.g., polyethylene terephthalate (PET)) in flexible, lightweight, eco-friendly solar cells [8–9], and light-emitting diodes (LEDs) [10–14]. Furthermore, cellulose-based materials can undergo modifications or treatments to acquire additional functionalities [15–17]. For instance, nanocellulose films present great haze, which have been proposed to scatter light and improve the performance of solar cell devices [18–20]. However, the literature has shown that this strategy could not be effective as expected when the angle of incidence of the light is higher than 30° [21]. Additionally, when the cellulose materials are surface modified by patterning, light diffraction or scattering leads to alteration of the light path [22–25]. Therefore, this approach of surface patterning can also be used for light management in solar cells [26].

Patterning can create optical effects depending on size, position, and shape. Figure 1 displays how different structural periods impact light and how the size of the structural period (Λ) about the wavelength of light (λ) defines the optical [27]: When the period size is minimal compared to the wavelength of light ($\lambda >> \Lambda$), minimal scattering occurs, and the surface provides anti-reflective properties. Conversely, when the structural size of the pattern is much larger than the wavelength of light ($\lambda << \Lambda$), the surface creates pronounced back and forward scattering. When the size of the structure is roughly equivalent to the wavelength of light ($\lambda \approx \Lambda$), the structure enables significant scattering in the forward direction [27]. If such a film ($\lambda \approx \Lambda$) is placed on top of a solar cell, the optical length in the solar cell increases, which enhances the likelihood of photon absorption, leading to an improvement in photocurrent and, therefore, in the overall performance [8,18,20].

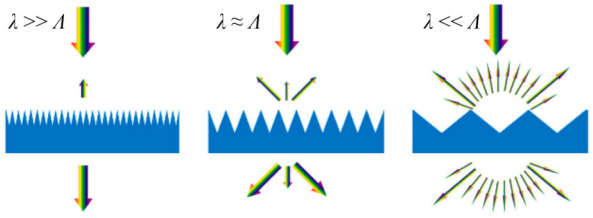

Fig. 1 Schematic illustrations of the optical effects induced by the periodically patterned surfaces of changing unique frequencies for a specific wavelength. λ is the wavelength and Λ is the structure period. Reproduced from Ref. [27] under an open-access Creative Common CC BY license (Copyright (2019) MDPI).

Different lithography techniques have been employed to pattern cellulose surfaces [11,22,28–30]. Depending on the chosen method, the chemical constitution of the films can either remain unaltered or change. For example, structured cellulose nanofiber and CA films fabricated using a vapor-assisted roll-to-roll imprinting technique [22–23,31] retained their chemical integrity after imprinting. In contrast, creating patterns through photolithography can lead to the chemical modification of cellulose [30]. Similarly, when soluble trimethylsilyl cellulose undergoes UV exposure, it converts into insoluble cellulose [32]. These insoluble cellulose patterns were employed in organic thin-film transistors, albeit with limited optical property evaluations. The added benefit of the soft nanoimprinting lithography (NIL) method is that it leaves the starting material unmodified. For example, the feasibility of using CA in NIL patterning of biological leaves was demonstrated [25].

Addressing challenges in light harnessing in some photovoltaic technologies, particularly dye-sensitized solar cells (DSSCs) and organic photovoltaics (OPVs), remains an important endeavor. DSSCs are a type of photovoltaic technology that has been inspired by photosynthesis and utilizes a light-absorbing dye instead of a conventional semiconductor. DSSCs comprise a photoanode with a dye sensitizer, an electrolyte with a reduction–oxidation (redox) couple, and a counter

electrode [33–34]. Their versatility extends to applications in building integration, consumer electronics, and transportation [35–37]. The conventional approach to increase light harvesting in dye solar cells has employed large light-reflecting particles in the TiO_2 layer. These approaches tend to increase the TiO_2 layer thickness and the potential sites for current leakage, which is problematic for many of the more recently studied high-performance electrolytes. Thus, exploring new approaches in material design and light management that allow thin TiO_2 layers is interesting. Modifying the photoelectrode substrate to support light harvesting is one such approach, and utilizing NIL is an easy and affordable method to pattern substrates to increase their optical function. Producing NIL films does not require specific temperature or vacuum conditions.

Furthermore, when NIL is employed for surface patterning, the chemical structure of the materials remains unchanged [38]. Its affordability and compatibility with a wide range of materials make it a promising selection for fabricating nanostructures. The NIL method requires a patterned mold usually made of polydimethylsiloxane (PDMS). PDMS is preferable for mold due to its flexibility, transparency, and low cost [39–40]. The NIL method does not require a clean room or other specialized devices, making it easily accessible to different laboratory settings. Furthermore, its affordability and compatibility with a wide range of materials make it a promising selection for fabricating nano- and microstructures. Additionally, there have been efforts in creating a pilot plant to produce lithography patterns, so large-scale production seems promising [22–23].

The novelty of this study is that we employed a fast and easy NIL method to fabricate nanostructures on CA films using a digital versatile disc (DVD) as a mold. We selected a DVD because, among the available patterns, this one could be easily used to produce patterns. Also, it provided approximately 800 nm structures in the range of DSSCs, which can utilize light and are close to the visible light range, where they are most efficient. The resulting nanostructured transparent CA films were applied as a light-scattering layer on top of DSSCs to extend the optical path length, thereby improving their efficiency. Scanning electron microscopy (SEM) and atomic force microscopy (AFM) were performed to determine the surface structure of the patterned CA film and h-PDMS mold. The transmittance and transmission haze of the CA films were measured with a UV–vis spectrophotometer. The enhancement in short-circuit current density and overall efficiency of the cells were measured under the solar simulator (1 Sun).

2 Experimental

2.1 Materials

CA (average Mn ≈ 50 000 $g \cdot mol^{-1}$ by gel permeation chromatography (GPC), 39.7 wt.% acetyl group, and average degree of substitution (DS) ≈ 1.2), acetone (99.5%), ethanol (99.9%), polyvinyl alcohol (PVA) (Mn = 30 000–70 000 $g \cdot mol^{-1}$, 87%–90% hydrolyzed), titanium (IV) chloride tetrahydrofuran (97%), TiO_2 paste transparent (791547), iodine (> 99.99%, trace metals), 1-methyl benzimidazole (99%), 1-methyl-3-propylimidazolium iodide (> 98%, high performance liquid chromatography (HPLC)), guanidine thiocyanate (for molecular biology > 99%), 3-methoxypropionitrile (> 98%, gas chromatography (GC)), Z907 ruthenium dye (95%, nuclear magnetic resonance spectroscopy (NMR)), 2 vol.% Hellmanex in distilled water (mild detergent), and chloroplatinic acid hydrate (~38% Pt basis) were bought from Sigma Aldrich. Sylgard 184 silicon elastomer base, Sylgard 184 elastomer curing agent, (7%–8% vinylmethylsiloxane)–(dimethylsiloxane) copolymer (Mn = 28 000 $g \cdot mol^{-1}$), 1,3,5,7-tetramethylcyclotetrasiloxane (TMCTS) (Mn = 240.51 $g \cdot mol^{-1}$), and platinum-divinyltetramethyldisiloxane (Mn = 474.68 $g \cdot mol^{-1}$) were bought from Dow Chemical Co., USA. Acetonitrile (> 99.9%) came from J.T. Baker, and tert-butanol (> 99%) from VWR. Fluorine-doped tin oxide (FTO) glass (2.5 mm, Pilkington TEC-15, sheet resistance 15 Ω/sq) was from Hartford Glass Company, Inc., while Surlyn 1702 foil was from DuPont.

2.2 Preparation of h-PDMS mold and patterned film

The preparation steps of PDMS used in pattern transfer are shown in Fig. 2. Firstly, h-PDMS, made out of 6.8 g of (7%–8% vinylmethylsiloxane)–(dimethylsiloxane) copolymer, 100 µL of TMCTS, 50 µL of platinum-divinyltetramethyldisiloxane, and 2 g of (25%–30% methylhydrosiloxane)–(dimethylsiloxane) copolymer were vigorously stirred resulting in a uniform h-PDMS slurry. Then, it was degassed in the vacuum oven for

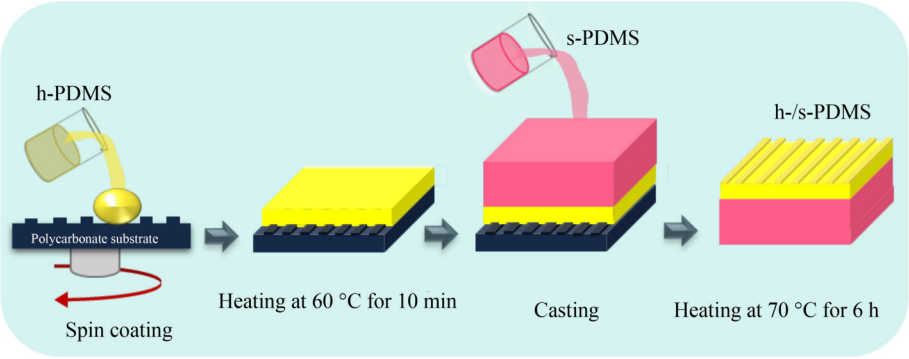

Fig. 2 Preparation of the patterned PMDS mold.

5 min at ambient temperature. The degassed h-PDMS was coated on a pre-patterned polycarbonate (PC) substrate via two-step spin coating at 500 $r \cdot min^{-1}$ for 5 s, followed by 1000 $r \cdot min^{-1}$ for 40 s. Afterwards, the h-PDMS/PC mold was heated in an oven at 60 °C for 10 min to cure the h-PDMS. Parallelly, the s-PDMS, made of Sylgard 184 base and its curing agent in a weight ratio of 10:1, was degassed in a vacuum oven for 10 min at ambient temperature. The s-PDMS was cast onto the h-PDMS/PC mold and heated at 70 °C for 6 h. Finally, the PC substrate (prepared from the DVD following the method in the work reported by Rodriguez et al. [41]) was carefully detached from the final mold.

A mixture of acetone and ethanol (9:1 (v/v)) was used to completely dissolve CA into a 10 wt.% solution. The patterned CA film was created by spin coating with 350 $r \cdot min^{-1}$ for 20 s on the mold and left to dry at room temperature for 20 min. The patterned CA film was peeled off from the surface of the PDMS mold. Also, the non-patterned CA film was created with the same concentration on a flat PDMS surface for comparison.

2.3 DSSC preparation

The photoelectrodes and counter electrodes in DSSCs were made on the FTO glasses, similar to those in our previous study [42]. After two electrodes had been sealed together, the electrolyte was injected through the small holes on the counter electrode substrate. The process of fabricating DSSCs involves several steps. First, FTO glasses were washed in an ultrasonic bath with different solvents of 2 vol.% Hellmanex solution, ethanol, and acetone for 10 min each. To prepare the photoelectrodes, the washed FTO glasses were immersed in a 1 wt.% solution of titanium(IV) chloride tetrahydrofuran in deionized water at 70 °C for 30 min to make a compact TiO_2 film, whose purpose was to suppress the charge recombination in the TiO_2 and electrolyte interface [43]. After the $TiCl_4$ treatment, a TiO_2 layer was deposited on FTO glasses using a doctor blade method with a microscopic slide and a commercially available TiO_2 paste. After sintering the TiO_2 layer at 450 °C for 30 min, the $TiCl_4$ treatment was repeated. Then, the photoelectrodes were immersed in a dye bath of 0.3 $mmol \cdot L^{-1}$ of Z907 ruthenium dye in a 1:1 solvent of acetonitrile and tert-butyl alcohol overnight.

To make the counter electrodes, a 4 μL solution of 10 $mmol \cdot L^{-1}$ H_2PtCl_6 in 2-propanol was applied to the washed FTO glasses, which (with the electrolyte filling holes) were heated at 390 °C for 15 min [42]. The electrolyte solution was composed of 0.05 $mol \cdot L^{-1}$ I_2, 0.5 $mol \cdot L^{-1}$ 1-methyl benzimidazole (NMBI), 0.5 $mol \cdot L^{-1}$ 1-methyl-3-propylimidazolium iodide (MPII), and 0.1 $mol \cdot L^{-1}$ guanidinium thiocyanate (GuSCN) in 3-methoxypropionitrile. The DSSCs were assembled by attaching the counter electrodes to photoelectrodes with Surlyn 1702 thermoplastic foil at 120 °C. 3 μL of electrolyte solution was applied to the assembled cells through a pre-drilled hole in the counter electrodes. The filling holes were closed using Surlyn 1702 foil and a thin cover glass. Copper tapes and silver paint were applied to contact areas, and epoxy was used to seal edges and protect the electrical connection. The patterned CA films (10 mm × 10 mm) were glued on top of the active area of DSSCs (8 mm × 4 mm) using 50 μL of 5 wt.% PVA in distilled water. The performance of the cells was measured after the CA film had completely been attached to the cell surface upon drying at room temperature.

2.4 Characterization of patterned CA film and DSSC performance

AFM (Bruker, Multimode) was used in tapping mode to determine the topography of the patterned CA film and PDMS mold surfaces. Images (10 μm × 10 μm) were obtained using the J scanner in the air. The AFM images were analyzed using the software Nanoscope analysis from BRUKER. The morphology of the patterned CA film and PDMS mold surfaces was also investigated using SEM (Thermo Scientific Apreo S). The transmittance and transmission haze were measured with a UV–vis spectrophotometer (UV-2600 spectrometer, Shimadzu Co., Japan) with ISR-2600 plus integrating sphere attachment in the wavelength range of 300–800 nm. The performance of the solar cells was evaluated using a solar simulator from Peccell (PEC-L01 No. 20Z0236) under conditions comparable to AM 1.5G standard testing. Current–voltage (*I–V*) measurement was conducted with 0.02 $V \cdot s^{-1}$ scan rate and 0.01 V step size using PalmSens4 potentiostat equipped with PSTrace software.

3 Results and discussion

3.1 Morphology of patterned CA film and PDMS mold

Using the NIL method, a PDMS mold was created for the two-dimensional (2D) structure on patterned CA film. A mixture of acetone and ethanol was utilized as the CA solvent during the spin coating process since acetone created bubbles and non-uniformities due to too rapid evaporation. The morphological properties of the mold and CA films were characterized using SEM. The SEM images show the highly uniform and repetitive structure on the surface of the mold and patterned CA film (Fig. 3), which confirms that the structure on the patterned CA film replicated the structure of the mold. The peak-to-peak distance is similar to the CA films and patterned mold: (750 ± 40) and (730 ± 30) nm, respectively. As mentioned before, the size of the mold and, thus, the patterned CA films were selected to create light scattering, which would then increase the optical path length in the solar device beneath the film [27]. To achieve this effect, the pattern and the usable light wavelengths should have similar sizes [8,18,20]. Here, the patterned film had the average periodic structure of (750 ± 40) nm, which aligns closely with the wavelength range of 300 to 800 nm that DSSCs mainly utilize.

The surface and mold were further analyzed with AFM (Fig. 4). The dimensions of the pattern on the mold and the CA film surfaces are exhibited in the height profiles shown in Figs. 4(c) and 4(d). Those show that the average peak-to-peak distance of nanostructures on the mold and the patterned CA film are (800 ± 30) and (830 ± 40) nm, respectively; thus, they are in the same magnitude as the values obtained from the SEM analysis. The height profile of the mold exhibits an average height of (76 ± 1) nm, while the patterned CA film has a (130 ± 7) nm average height. The order of magnitude in the heights is similar for the patterned CA film and PDMS mold, and these results show the feasibility of pattern translation. In previous literature, there are also some height differences between molds and cellulose materials, which are attributed to factors related to processing temperature and material properties [29,44].

3.2 Optical analysis of patterned and non-patterned CA films

Transparency and transmission haze are key for optoelectronic devices, affecting performance and appearance. High transparency of the substrates is mandatory for good performance of solar cells.

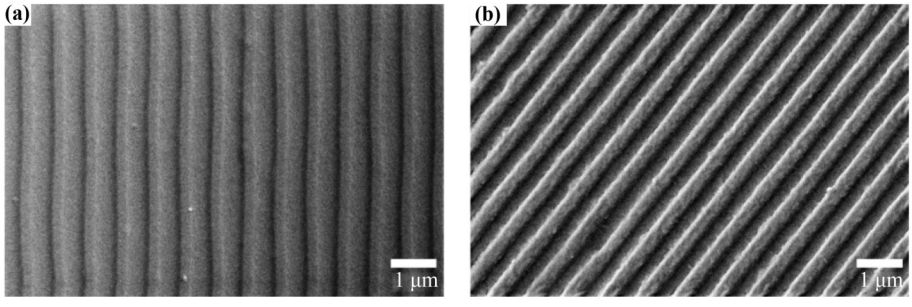

Fig. 3 SEM images of (**a**) mold and (**b**) patterned CA films.

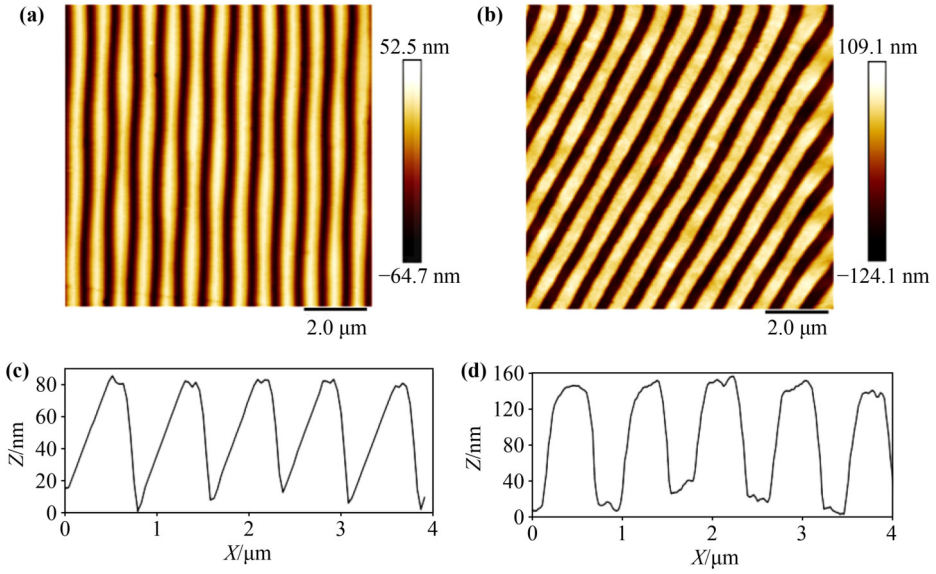

Fig. 4 AFM images of (**a**) mold and (**b**) patterned CA films. Height profiles of diagonal cross-sections for (**c**) mold and (**d**) patterned CA films.

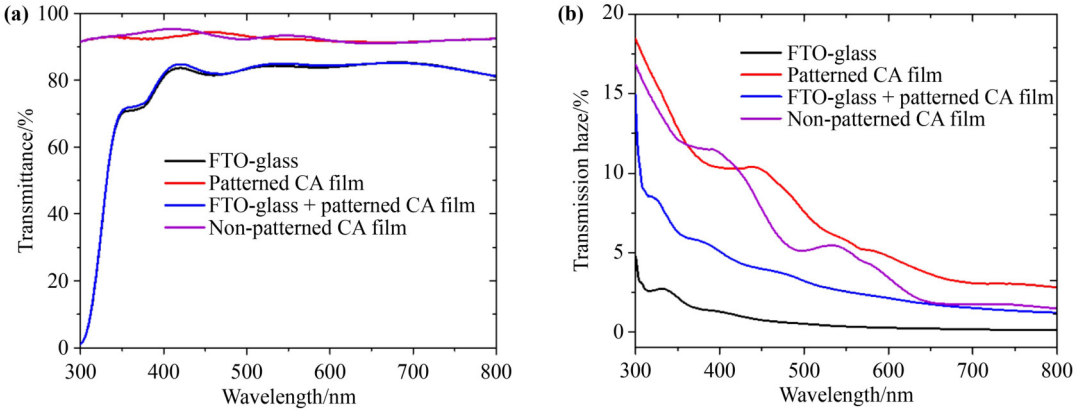

Fig. 5 (**a**) Transmittance spectra and (**b**) corresponding haze spectra of FTO-glass, pattern CA film, pattern CA film attached to FTO-glass, and non-patterned CA film.

Transmission haze refers to the fraction of diffusely scattered light to the total transmitted light through a transparent surface. It has been suggested that increased scattering caused by high transmission haze could extend the optical path length in the following layer [8,18,20]. A longer optical path in solar cells results in improved light absorption by active materials, increasing the short circuit current and, consecutively, the power conversion efficiency. Figure 5 presents the transmittance and the transmission haze in the wavelength range between 300 and 800 nm for non-patterned CA film, patterned CA films, FTO glass, and patterned CA film attached to the glass.

As shown in Fig. 5(a), the transmittance of both the non-patterned and patterned CA films exceeds 90%, exhibiting similar trends in the visible light wavelengths range. This similarity is expected due to the identical production method and the same concentration of the CA solution used for both types of CA films. The films made of cellulose derivatives, such as CA, are homogeneous and can reach high transparency because of the low chemical absorption and the low reflective surface in the wavelength ranging from 380 to 870 nm [1,45]. The transmittance for the non-patterned and patterned CA films is more than 90% (Fig. 5(a)). Adding the CA film on top of the FTO glass slightly improved the transmission (approximately 1%) compared to the bare FTO glass (80%) (Fig. 5(a)). This enhancement results from the CA film's refractive index (1.47) [46], which lies between air (1) and glass (1.51), reducing reflection. To

attach the CA film to the DSSCs, we used PVA, as its refractive index (1.477) closely matches the CA refractive index and efficiently penetrates the film acting as glue. An air gap would form without adhesive, causing a backing reflection and lowering the transmittance. Additionally, FTO glass has high transparency in the wavelength range of 400–800 nm due to its wide band gap [35,47], and it blocks light in wavelengths below 350 nm [48–50].

The haze in cellulose films can be increased by modifying physical parameters such as thickness, density, and surface morphology by applying modifications to the preparation method [51–52]. Both non-patterned and patterned CA films exhibit higher haze in short wavelength ranges, especially between 300 and 500 nm, compared to the glass samples, as Fig. 5(b) shows. While in most studied wavelengths, the patterned surface reached higher haze compared to the non-patterned one, as to be expected, it is surprising that the difference was not more significant. It should be noted that DSSCs usually harvest low wavelengths efficiently; thus, extending the optical path, particularly in the higher wavelengths, is essential.

3.3 Measuring performance of DSSCs

The efficiency of DSSCs was measured before and after attaching the CA films (Table 1), and Fig. 6 shows an example of the *I*–*V* curve.

The photovoltaic parameter is V_{oc}, which provides the maximum voltage available for the solar cell at the open circuit; J_{sc} presents the current density through the solar cell when the voltage across the cell is zero; fill factor (FF), and efficiency (η) [33,53]. The optical film is aimed to increase, namely J_{sc}, and indeed, there is a significant improvement (17%), as shown in Table 1. The other main characteristics, V_{oc} and FF, remain unchanged, which is expected since, for instance, FF changes arise from internal resistances [54]. The 17% increase in J_{sc} creates a similar improvement in η. The improvements in J_{sc} and η are relatively significant compared to the haze the patterned film created. Thus, the performance may receive an additional boost due to changes in the light path and refractive index variations introduced by the combination of materials used in the cell structure (patterned CA film, PVA glue, and glass). A detailed investigation of this effect would require extensive computational analysis, which is beyond the scope of this study.

A recently published work explores the translation of biological leaf patterns on CA films used on top of perovskite solar cells, increasing the efficiency by 6% [25]. It should be noted that efficiency improvement is also related to the many challenges they face in light harvesting. Thus, the improvement efficiency in different device types is insufficient for comparison. In that study, the anisotropic self-cleaning functionality was optimized with some optical improvements [25]. The results in this current work support the idea that patterned cellulose acetate film can be used versatilely to improve functionalities, notably the light management of emerging solar cells. Compared to leek leave replicas, with repeating structures in μm scale, the patterned surface structure in this work is more regular, and the groove-to-groove distance is smaller. While both structures were beneficial for photovoltaic add-on layers, the structure demonstrated here is closer to the wavelengths of visible light, which are more efficiently harvested by DSSCs. Our future work involves replacing the actual glass supports

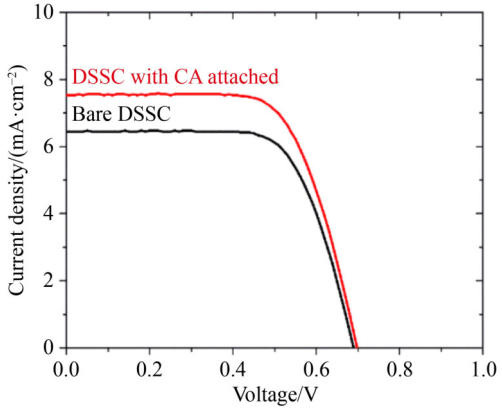

Fig. 6 *I*–*V* curves of example devices: a bare DSSC (black) and a DSSC with patterned CA attached (red).

Table 1 Photovoltaic parameters of the bare solar cell with CA film (each data averages four cells)

DSSC	η/% a)	J_{sc}/(mA·cm^{-2}) b)	V_{oc}/mV c)	FF/% d)
Bare solar cell	2.9 ± 0.4	6.5 ± 0.3	700 ± 9	65 ± 9
Solar cell with CA attached	3.4 ± 0.4	7.6 ± 0.4	708 ± 9	64 ± 6

a) η, overall conversion efficiency; b) J_{sc}, short circuit current density; c) V_{oc}, open circuit voltage; d) FF, fill factor.
Note: The enhancement ratios of η, J_{sc}, V_{oc}, and FF for solar cells attached with CA compared to those for bare solar cells are 17%, 17%, 1%, and −2%, respectively.

with patterned cellulose-based substrates to create more sustainable and easy-to-recycle emerging photovoltaics [25,55–56].

4 Conclusion

In this work, the nanostructured pattern of the DV disc was translated into the CA films using the NIL technique. The patterned CA films achieved high transmittance (more than 90%) and created some transmission haze over the studied wavelength range (300–800 nm). The patterned CA film was used as the scattering layer atop DSSCs, improving their efficiency. The DSSCs with the CA films had 17% higher short circuit current density (from 6.5 to 7.6 $mA \cdot cm^{-2}$), causing a consequent increase of average energy conversion efficiency by 17% (from 2.9% to 3.4%). As compared to previous literature, the employed method is highly cost-effective and accessible, not requiring any access to clean room environments or specialized equipment. We also highlight that this patterning technique is not limited to specific solar cell types but could apply to light management for other optoelectronic devices. Furthermore, cellulose acetate is more hydrophobic than other cellulose films, and it allows easy modification, enabling the combination of surface patterning with other functionalities inside the film, such as spectral management and UV protection.

Authors' contributions Conceptualization: J.K., J.V., and K.M. Methodology: J.K. — materials; J.V. — soft lithography approach; H.N. — replication; K.M. — testing in solar cells. Formal analysis: K.M., J.K., J.V., and M.E. Investigation: M.E. — main work; Y.A. — optical measurements; H.N. — AFM images. Writing: M.E. — original draft; K.M., J.K., J.V., and E.P. — review & editing significant contributions; other authors — review & edit minor contributions. Supervision: K.M. — overall; J.K. and J.V. — soft lithography; H.N. — making patterned PDMS molds. Funding acquisition: K.M., J.V., and M.E.

Declaration of competing interests The authors declare no conflict of interests.

Acknowledgements This work was a part of the Academy of Finland's Flagship Program under Projects Nos. 318890 and 318891 (Competence Center for Materials Bioeconomy, FinnCERES). M.E., J.V., and K.M. acknowledge the Academy of Finland projects "SUSTAINABLE" and BioEST (Decision numbers 334818, 334819, 336577, and 336441) for funding. M.E. also thanks the Graduate School of the University of Turku. We acknowledge the use of UTU's Materials Research Infrastructure (MARI).

References

[1] Kaschuk J J, Al Haj Y, Rojas O J, et al. Plant-based structures as an opportunity to engineer optical functions in next-generation light management. Advanced Materials, 2022, 34(6): 2104473

[2] Kaschuk J J, Borghei M, Solin K, et al. Cross-linked and surface-modified cellulose acetate as a cover layer for paper-based electrochromic devices. ACS Applied Polymer Materials, 2021, 3(5): 2393−2401

[3] Miettunen K, Hadadian M, García J V, et al. Bio-based materials for solar cells. Wiley Interdisciplinary Reviews: Energy and Environment, 2024, 13(1): e508

[4] Nizamov R, Kaschuk J, Al Haj Y, et al. Optical assessment of lignin-containing nanocellulose films under extended sunlight exposure. Cellulose, 2025 (in press) doi:10.1007/s10570-025-06380-7

[5] Kaschuk J J, Miettunen K, Borghei M, et al. Electrolyte membranes based on ultrafine fibers of acetylated cellulose for improved and long-lasting dye-sensitized solar cells. Cellulose, 2019, 26(10): 6151−6163

[6] Khoshnevisan K, Maleki H, Samadian H, et al. Cellulose acetate electrospun nanofibers for drug delivery systems: applications and recent advances. Carbohydrate Polymers, 2018, 198: 131−141

[7] Liu H Q, Tang C Y. Electrospinning of cellulose acetate in solvent mixture *N,N*-dimethylacetamide (DMAc)/acetone. Polymer Journal, 2007, 39(1): 65−72

[8] Zhou Y H, Fuentes-Hernandez C, Khan T M, et al. Recyclable organic solar cells on cellulose nanocrystal substrates. Scientific Reports, 2013, 3: 1536

[9] Fang Z Q, Zhu H L, Li Y Y, et al. Light management in flexible glass by wood cellulose coating. Scientific Reports, 2014, 4: 5842

[10] Legnani C, Barud H S, Caiut J M A, et al. Transparent bacterial cellulose nanocomposites used as substrate for organic light-emitting diodes. Journal of Materials Science: Materials in Electronics, 2019, 30(18): 16718−16723

[11] Jürgensen N, Fritz B, Mertens A, et al. A single-step hot embossing process for integration of microlens arrays in biodegradable substrates for improved light extraction of light-emitting devices. Advanced Materials Technologies, 2021, 6(2): 1900933

[12] Zhou S, Wan Z, Lei Y, et al. InGaN quantum well with gradually varying indium content for high-efficiency GaN-based green light-emitting diodes. Optics Letters, 2022, 47(5): 1291−1294

[13] Cui S Y, Sun K, Liao Z F, et al. Flexible nanoimprint lithography enables high-throughput manufacturing of bioinspired microstructures on warped substrates for efficient III-nitride optoelectronic devices. Science Bulletin, 2024, 69(13): 2080−2088

[14] Zhou S, Zhao X, Du P, et al. Application of patterned sapphire

substrate for III-nitride light-emitting diodes. Nanoscale, 2022, 14(13): 4887−4907

[15] Reimer M, Zollfrank C. Cellulose for light manipulation: methods, applications, and prospects. Advanced Energy Materials, 2021, 11(43): 2003866

[16] Chen S, Song Y, Xu F. Highly transparent and hazy cellulose nanopaper simultaneously with a self-cleaning superhydrophobic surface. ACS Sustainable Chemistry & Engineering, 2018, 6(4): 5173−5181

[17] Qiu C J, Liu H C, Shen K Y, et al. Rational design of stable fluorescent and hydrophobic cellulose-based film for full-band UV-blocking. Cellulose, 2022, 29(18): 9719−9729

[18] Fang Z, Zhu H, Yuan Y, et al. Novel nanostructured paper with ultrahigh transparency and ultrahigh haze for solar cells. Nano Letters, 2014, 14(2): 765−773

[19] Jia C, Li T, Chen C J, et al. Scalable, anisotropic transparent paper directly from wood for light management in solar cells. Nano Energy, 2017, 36: 366−373

[20] Ha D, Fang Z, Hu L, et al. Paper-based anti-reflection coatings for photovoltaics. Advanced Energy Materials, 2014, 4(9): 1301804

[21] Kaschuk J J, Al Haj Y, Valdez Garcia J, et al. Processing factors affecting roughness, optical and mechanical properties of nanocellulose films for optoelectronics. Carbohydrate Polymers, 2024, 332: 121877

[22] Mäkelä T, Hokkanen A, Sneck A, et al. Vapour-assisted roll-to-roll nanoimprinting of micropillars on nanocellulose films. Microelectronic Engineering, 2020, 225: 111258

[23] Mäkelä T, Kainlauri M, Willberg-Keyriläinen P, et al. Fabrication of micropillars on nanocellulose films using a roll-to-roll nanoimprinting method. Microelectronic Engineering, 2016, 163: 1−6

[24] Banvillet G, Pritchard S, Kaschuk J J, et al. Monolithic nanocellulose films patterned with flower-shaped and other microstructures: a facile route to modulate topographical, wetting and optical properties. Materials Today Nano, 2023, 24: 100424

[25] Daghigh Shirazi H, Mirmohammadi S M, Mousavi S M, et al. Bio-inspired surface structures promote optical transmittance and hydrophobicity in cellulose-based films for self-cleaning perovskite solar cells. Communications Materials, 2024, 5(1): 88

[26] Kim M S, Lee J H, Kwak M K. Review: surface texturing methods for solar cell efficiency enhancement. International Journal of Precision Engineering and Manufacturing, 2020, 21(7): 1389−1398

[27] Amalathas A P, Alkaisi M M. Nanostructures for light trapping in thin film solar cells. Micromachines, 2019, 10(9): 619

[28] Takei S, Oshima A, Wakabayashi T, et al. Eco-friendly electron beam lithography using water-developable resist material derived from biomass. Applied Physics Letters, 2012, 101: 033106

[29] Espinha A, Dore C, Matricardi C, et al. Hydroxypropyl cellulose photonic architectures by soft nanoimprinting lithography. Nature Photonics, 2018, 12(6): 343−348

[30] Wolfberger A, Petritz A, Fian A, et al. Photolithographic patterning of cellulose: a versatile dual-tone photoresist for advanced applications. Cellulose, 2015, 22(1): 717−727

[31] Mäkelä T, Haatainen T, Ahopelto J. Roll-to-roll printed gratings in cellulose acetate web using novel nanoimprinting device. Microelectronic Engineering, 2011, 88(8): 2045−2047

[32] Li Y Y, Yu S, Veinot J G C, et al. Luminescent transparent wood. Advanced Optical Materials, 2017, 5(1): 1600834

[33] Hagfeldt A, Boschloo G, Sun L, et al. Dye-sensitized solar cells. Chemical Reviews, 2010, 110(11): 6595−6663

[34] Grätzel M. Conversion of sunlight to electric power by nanocrystalline dye-sensitized solar cells. Journal of Photochemistry and Photobiology A: Chemistry, 2004, 164(1−3): 3−14

[35] Bandara T M W J, Hansadi J M C, Bella F. A review of textile dye-sensitized solar cells for wearable electronics. Ionics, 2022, 28: 2563−2583

[36] Aslam A, Mehmood U, Arshad M H, et al. Dye-sensitized solar cells (DSSCs) as a potential photovoltaic technology for the self-powered internet of things (IoTs) applications. Solar Energy, 2020, 207: 874−892

[37] Venkatesan S, Lin W H, Teng H S, et al. High-efficiency bifacial dye-sensitized solar cells for application under indoor light conditions. ACS Applied Materials & Interfaces, 2019, 11(45): 42780−42789

[38] Guo L J. Nanoimprint lithography: methods and material requirements. Advanced Materials, 2007, 19(4): 495−513

[39] Choi K M, Rogers J A. A photocurable poly(dimethylsiloxane) chemistry designed for soft lithographic molding and printing in the nanometer regime. Journal of the American Chemical Society, 2003, 125(14): 4060−4061

[40] Bhingardive V, Menahem L, Schvartzman M. Soft thermal nanoimprint lithography using a nanocomposite mold. Nano Research, 2018, 11(5): 2705−2714

[41] Rodriguez I, Fenollosa R, Ramiro-Manzano F, et al. Groove-assisted solution growth of lead bromide perovskite aligned nanowires: a simple method towards photoluminescent materials with guiding light properties. Materials Chemistry Frontiers, 2019, 3(9): 1754−1760

[42] Poskela A, Miettunen K, Borghei M, et al. Nanocellulose and nanochitin cryogels improve the efficiency of dye solar cells. ACS Sustainable Chemistry & Engineering, 2019, 7(12): 10257

[43] Sharif N F M, Shafie S, Ab Kadir M Z A, et al. The effect of titanium(IV) chloride surface treatment to enhance charge transport and performance of dye-sensitized solar cell. Results in Physics, 2019, 15: 102725

[44] Baek W H, Seo I, Yoon T S, et al. Hybrid inverted bulk heterojunction solar cells with nanoimprinted TiO_2 nanopores. Solar Energy Materials and Solar Cells, 2009, 93(9): 1587−1591

[45] Orelma H, Hokkanen A, Leppänen I, et al. Optical cellulose fiber made from regenerated cellulose and cellulose acetate for water sensor applications. Cellulose, 2020, 27(3): 1543−1553

[46] Kasarova S N, Sultanova N G, Ivanov C D, et al. Analysis of the dispersion of optical plastic materials. Optical Materials, 2007, 29(11): 1481−1490

[47] Banyamin Z Y, Kelly P J, West G, et al. Electrical and optical properties of fluorine doped tin oxide thin films prepared by magnetron sputtering. Coatings, 2014, 4(4): 732−746

[48] Shanthi S, Anuratha H, Subramanian C, et al. Effect of fluorine doping on structural, electrical and optical properties of sprayed SnO_2 thin films. Journal of Crystal Growth, 1998, 194(3−4): 369−373

[49] Supriyono, Surahman H, Krisnandi Y K, et al. Preparation and characterization of transparent conductive SnO_2-F thin film deposited by spray pyrolysis: relationship between loading level and some physical properties. Procedia Environmental Sciences, 2015, 28: 242−251

[50] Gutierrez J, Carrasco-Hernandez S, Barud H S, et al. Transparent nanostructured cellulose acetate films based on the self assembly of PEO-b-PPO-b-PEO block copolymer. Carbohydrate Polymers, 2017, 165: 437−443

[51] Kim Y, Song Y, Kim H. Preparation of transparent cellulose film with controlled haze using halloysite nanotubes. Cellulose, 2018, 25(2): 1239−1248

[52] Lin C M, Wang Q H, Deng Q D, et al. Preparation of highly hazy transparent cellulose film from dissolving pulp. Cellulose, 2019, 26(6): 4061−4069

[53] Qi B Y, Wang J Z. Fill factor in organic solar cells. Physical Chemistry Chemical Physics, 2013, 15(23): 8972−8982

[54] Halme J, Vahermaa P, Miettunen K, et al. Device physics of dye solar cells. Advanced Materials, 2010, 22(35): E210−E234

[55] Akulenko E S, Hadadian M, Santasalo-Aarnio A, et al. Eco-design for perovskite solar cells to address future waste challenges and recover valuable materials. Heliyon, 2023, 9(2): e13584

[56] Miettunen K, Santasalo-Aarnio A. Eco-design for dye solar cells: From hazardous waste to profitable recovery. Journal of Cleaner Production, 2021, 320: 128743